Title:

Receptor interacting protein kinase-3 promotes both myopathy and cardiomyopathy in dystrophin-deficient mice

Running title: Necroptosis mediates both myopathy and cardiomyopathy in DMD

Maximilien Bencze[1] ✉ , Cyrielle Hou[1], Baptiste Periou[1], Onnik Agbulut [2], Marianne Gervais[1], Julien Ternacle[3], Geneviève Derumeaux[3], Laurent Tiret[1], Fréderic Relaix[1], François-Jérôme Authier[1]

[1] U955-IMRB, Inserm, UPEC, ENVA, EFS, Team 10, Biology of the Neuromuscular System, Créteil 94000, France.

[2] Sorbonne Université, Institut de Biologie Paris-Seine (IBPS), CNRS UMR 8256, Inserm ERL U1164, Biological Adaptation and Ageing, 75005, Paris-France.

[3] U955-IMRB, Université Paris-Est Créteil (UPEC), Team 8, Department of Physiology, Henri Mondor Hospital, FHU-SENEC, AP-HP, Créteil, France.

✉ **Correspondence:** Maximilien Bencze: maximilien.bencze@inserm.fr

Keywords: Duchenne muscular dystrophy, myonecrosis, necroptosis, myogenesis, cardiomyopathy, fibrosis.

Abstract

Background

Duchenne muscular dystrophy (DMD) is a muscle degenerative disorder that is caused by the absence of dystrophin. From early childhood, multiple rounds of myofibre necrosis and regeneration lead to fibrosis and fat deposition, irreversibly disturbing skeletal muscle function and impairing locomotion. Cell necrosis also affects respiratory muscles and cardiomyocytes, ultimately responsible for the death of DMD boys by respiratory or heart failure.

Necroptosis is a genetically programmed form of necrosis requiring the receptor-interacting serine/threonine-protein kinase (RIPK)3 and is a promising new therapeutic target for multiple degenerative disorders. We previously demonstrated that necroptosis mediates hindlimb myofibre degeneration in distinct muscular dystrophies, including in DMD. However, this pathway was recently found to be required for myogenesis. Its prevention might therefore lead to detrimental side effects on muscle repair.

Whether necroptosis also participates in the pathogenesis of respiratory and cardiac muscle dysfunction, and whether its long-term inhibition would ultimately be beneficial or detrimental to mdx mice are addressed here.

Methods

Herein, we examined the effects of RIPK3 depletion on an advanced stage of pathogenesis in mdx mice. Dystrophic mice aged 12 to 18 months were submitted to forced treadmill running to assess their locomotor function. mdx cardiomyopathy was also examined by echocardiography in 40-week-old mice. Limb skeletal muscles, diaphragm and heart were analyzed by histology and molecular biology to compare the phenotype of mdx*Ripk3*$^{+/+}$ mdx*Ripk3*$^{-/-}$ mice.

Results

In 18-month-old mdx*Ripk3*$^{-/-}$ mice, we found no sign of muscle regeneration defect compared to mdx*Ripk3*$^{+/+}$ littermates. mdx*Ripk3*$^{-/-}$ mice had decreased fibrosis in limb muscles, without evidence of muscle atrophy. The size of diaphragm myofibres was slightly reduced and affected by less variability than mdx littermates. Fibrosis was also reduced in the diaphragm of RIPK3-deficient mdx mice. Notably, heart hypertrophy and left ventricle fibrosis were reduced in mdx*Ripk3*$^{-/-}$ mice, and using

echocardiography, we found a significant decrease of markers of cardiomyopathy by such as a reduction of the relative wall thickness and left ventricle mass.

Conclusions

Our data suggest that necroptosis is involved together in the pathogenic phenotype of locomotor, respiratory, and cardiac muscles in dystrophin-deficient mice. The long-term genetic ablation of RIPK3 does not generate evidence of sarcopenia or muscle impairment in mdx mice. Our data suggest that necroptosis may represent a new therapeutic target susceptible to improving the phenotype of myopathy and cardiomyopathy.

Introduction

Duchenne muscular dystrophy (DMD) is an X-linked genetic disorder, affecting 1/5000 male birth worldwide. Loss-of-function mutations in the dystrophin gene primarily lead to chronic myofiber necrosis (myonecrosis) and severe locomotor muscle disability starting in early childhood (Gilbert and Hawk, 1963)(Duan et al., 2021). Notably, the absence of dystrophin at the sarcolemma renders myofibre less resistant to mechanical stress during muscle contraction, which favours myonecrosis. Following injury, muscle repair requires myogenesis thanks to the contribution of PAX7-expressing resident muscle stem cells (MuSC). (For review, see Relaix et al., 2021). However, in disabling neuromuscular disorders involving chronic myofiber degeneration such as DMD, regeneration does not fully compensate for chronic myofibre demise and loss of a sustained homeostatic balance between the two mechanisms leads to the increasing replacement of contractile myofibres by fibrotic or adipose tissue. Indeed, biopsies with interstitial fibrosis positively correlate with a poor outcome in DMD boys (Desguerre et al., 2009), and thus identifying the molecular pathways involved in fibrosis formation is relevant for improving therapeutic perspectives. Dystrophin deficiency also targets respiratory and cardiac muscle cells that are prone to precocious necrotic cell death, ultimately leading to the premature death of DMD patient from cardiorespiratory weakness or failure (Khirani et al., 2014)(Fayssoil et al., 2017).

Recently, we reported that canonical necroptosis, a receptor-interacting protein kinase (RIPK)1- RIPK3- and mixed lineage domain kinase-like (MLKL)-dependent cell death pathway, is activated in the human and murine dystrophin-deficient muscles. Necroptosis inhibition dampens the peak of myonecrosis in the locomotor muscles of three-week-old mdx mice and improves muscle function in young adults (Morgan et al., 2018). Before further envisaging the necroptotic pathway as a putative therapeutic target for DMD, several key questions need to be addressed, including the long-term effects of necroptosis inhibition in dystrophic skeletal and heart muscle remodeling. Indeed, two distinct and recent studies reported a link between necroptosis inhibition and a deficit in myogenesis (Sreenivasan et al., 2020)(Zhou et al., 2020a), and one of them reported that RIPK3 depletion in mdx MuSCs dramatically impaired muscle function. Repressing necroptosis might therefore lead to two putative conflictual

83 outcomes: a decrease in myofiber degeneration together with a default in muscle regeneration leading
84 to atrophy.
85 In this context, the present study aimed at investigating *in vivo* the long-term effects of necroptosis
86 inhibition on the most affected tissues in mdx mice: hindlimb muscles, the diaphragm, and the heart.
87 We found that RIPK3 depletion did not reduce the running performance of old mdx mice. Compared to
88 mdx*Ripk3*$^{+/+}$, locomotor muscles from mdx*Ripk3*$^{-/-}$ mice displayed no evidence of regenerative default,
89 i.e. muscles had similar cell proliferation, MuSCs content, myogenic commitment, and myofibre size.
90 On the long term, RIPK3 depletion also led to a significant reduction of fibrosis in the diaphragm, and
91 reduced the mean myofibre size and their variability, indicating that necroptosis not only participates in
92 the pathology of limb, but also of respiratory muscles. Importantly, we found a beneficial effect of
93 RIPK3 depletion on cardiomyopathy in aged mdx mice by reducing heart hypertrophy and fibrosis
94 deposition. Together, our data demonstrate that in our mdx model, RIPK3 is dispensable for long term
95 post-lesional myogenesis, suggest that necroptosis inhibition would together benefit hindlimb,
96 respiratory, and heart muscles in dystrophinopathies and prompt further analyses to explore the
97 therapeutic benefit of reducing necroptosis to improve patients' living conditions.

98 # Results

99 Although RIPK3-dependant necroptosis is implicated in early mdx myofiber death (Morgan et al.,
100 2018), its specific depletion in MuSCs was recently described to induce PAX7-positive cells death and
101 a subsequent deficit in myogenesis, causing a dramatically reduced muscle strength in adult mdx mice
102 (Sreenivasan et al., 2020). We thus examined whether the long-term genetic inhibition of necroptosis
103 would promote sarcopenia by repressing the regenerative capacity of skeletal muscle. mdx mice were
104 crossed with *Ripk*3-KO mice, which are compromised for RIPK3-dependent necroptosis (Newton et al.,
105 2004). We generated mdx*Ripk3*$^{+/+}$ (hereafter named mdx*Ripk3*$^{+/+}$ or mdx) and mdx*Ripk3*$^{-/-}$ littermates
106 that were kept for ageing so that the maximum mdx pathogenic state could be reached for striated
107 muscles. In 18-month-old mdx*Ripk3*$^{-/-}$ mice, *Ripk1* transcripts were downregulated in muscles compared
108 to *Ripk3*$^{+/+}$ littermates (Figure 1a), assessing that canonical necroptosis is repressed in our mdx*Ripk3*$^{-/-}$
109 mice. Seventeen-month-old mdx and mdx*Ripk3*$^{-/-}$ littermates were submitted to forced treadmill exercise

110 with progressive increase of speed, until exhaustion. Control mdx mice were characterized by an
111 important variability in running performance, expressed in the running distance (Figure 1b) or in the
112 maximum aerobic speed before exhaustion (Figure 1c). mdx*Ripk3*$^{-/-}$ mice showed more homogenous
113 results (coefficient of variation: mdx:20,99% *versus* mdx*Ripk3*$^{-/-}$ 12.66%). On average, mdx*Ripk3*$^{-/-}$ ran
114 ~ 10% longer than mdx littermates, despite no statistical difference likely due to the variability of control
115 mdx phenotype (p=0.5530). Atrophy of dystrophic muscles was investigated using muscle mass
116 normalized to the individual size of the animals, assessed by the *tibialis anterior* length (TL). TA, EDL
117 and biceps muscle mass remained unchanged in aged mdx*Ripk3*$^{-/-}$ compared to mdx*Ripk3*$^{+/+}$ mice
118 (Figure 1d). In the few post-necrotic areas we spotted in TAs of old mdx, we found a similar density of
119 Ki67-positive cells (Figure 1e,f) suggesting that necroptosis inhibition does not significantly affect
120 MuSC proliferation in mdx muscle. The mean of pooled minimum Feret of TA myofibres (Figure 1g),
121 as well as the relative distribution of myofiber size (Figure 1h), were strictly unchanged. Interestingly,
122 we found that RIPK3 depletion reduced fibrosis in the TA (p=0.0252) (Figure 1m), suggesting a benefit
123 for mdx limb muscle phenotype.
124 To further examine any possible evidence of regenerative default in mdx*Ripk3*$^{-/-}$ muscles, we analyzed
125 biceps muscles by molecular biology. We found normal expression of *Pax7* (Figure 1i) and *myogenin*
126 (Figure 1j), indicating that in this model the long-term inhibition of necroptosis generated neither muscle
127 atrophy nor decreased the number of MuSCs and their myogenic commitment. Of note, we observed a
128 significant downregulation of *myostatin* expression (p=0.0082), while *follistatin* was not significantly
129 repressed (p=0.4452) (Figure 1k,l).
130 Fibrosis deposition in respiratory muscles, such as the diaphragm, is also a key pathogenic event in
131 DMD pathogenesis and is a major cause of patient's death. We then investigated the effects of RIPK3
132 depletion in the phenotype of the mdx diaphragm (Figure 2). We previously reported that at the onset of
133 pathogenesis in mdx, occurring at around three weeks of age, TA from mdx*Ripk3*$^{-/-}$ mice display a
134 reduced myonecrosis, but much less at mdx adulthood when myonecrosis becomes rare (Morgan et al.,
135 2018). IgG uptake within sarcoplasm is a reliable readout for ongoing myonecrosis in young mdx
136 (Straub et al., 1997)(Bencze et al., 2019). In contrast with what was observed in wild-type or less
137 affected muscles from young animals, mouse IgG immunoreactivity is almost only localized at the

138 extracellular compartment (Figure 2a), and no difference was found in both genotypes (unpaired t-test,
139 p=0.1914). The density of fibres with leaky sarcolemma was extremely low in both genotypes (2.3
140 fibres/mm^2 in mdx versus 2.6 fibres/mm^2 in mdx*Ripk3*$^{-/-}$) (Figure 2b,c). This was neither associated with
141 high-density cell pockets (Figure 2d) nor with CD68-positive cell infiltrates (Figure 2e). Furthermore,
142 only a low percentage of centrally nucleated fibres was found in mdx diaphragms (5-10% of myofibers)
143 (Figure 2f). These observations suggest that diaphragm from 18-month-old mdx mice stand at relative
144 homeostasis with little/no ongoing myonecrosis, regardless of RIPK3 expression. Examining the profile
145 of myofibre size, we observed a moderate decrease of myofibre size in mdx*Ripk3*$^{-/-}$ diaphragm compared
146 to mdx littermates (16.6 in mdx versus 16.1 in mdx*Ripk3*$^{-/-}$, p<0.0001, Mann Whitney test, n>16,000
147 myofibers in each group, included in six mdx muscles, and eight mdx*Ripk3*$^{-/-}$ muscles). Of note,
148 myofibre size is meant to be increased in the mdx diaphragm. Dystrophin-deficient muscles are
149 characterized by an increased heterogeneity in myofiber size, illustrated by an increase of the variance
150 coefficient (Briguet et al., 2004). *Ripk3* deficiency decreased the mean-variance coefficient of myofibers
151 in mdx mice (Figure 3i, unpaired t-test p=0.0431). To determine whether RIPK3 also mediates fibrosis
152 deposition in the diaphragm, muscle sections were stained with Sirius red (Figure 3k), and we quantified
153 that mdx*Ripk3*$^{-/-}$ diaphragms had less collagen deposition than mdx littermates (Figure 3k, unpaired
154 t-test, p=0.0414). Together, our data demonstrate that RIPK3 participates in the diaphragm remodeling
155 and that its depletion reduces both the size impairment of dystrophic myofibres and the interstitial
156 fibrosis.
157 Dilated cardiomyopathy, associated with hallmarks of focal degeneration and fibrosis, is a major
158 concern in DMD patients. The cell death pathway(s) responsible for the loss of dystrophin-deficient
159 cardiomyocytes has not yet been identified, but necroptotic demise has been identified in several models
160 of heart injuries (Zhe-Wei et al., 2018). We then addressed the role of necroptosis in the long-term
161 development of cardiomyopathy in mdx mice.
162 Notably, we quantified that RIPK3 depletion decreased cardiac hypertrophy in mdx mice, regardless of
163 their size (Figure 3a, b). The mdx heart from 18-month-old mice showed no significant level of ongoing
164 degeneration, with little CD68-positive cells infiltration in both genotypes (Figure 3c). By contrast, we
165 quantified a decrease in cardiac capillarization (Figure 3d), and interstitial collagen deposition was

166 reduced by almost 50% in the right ventricle of mdx*Ripk3*$^{-/-}$ mice compared to their mdx control
167 littermates (Figure 3e,f). Furthermore, mdx*Ripk3*$^{-/-}$ hearts showed significantly reduced levels of *Bnp*
168 and *Myf7* transcripts that are two sensitive markers of cardiac hypertrophy (Figure 3g).
169 We thus examined whether the improvement of the deleterious phenotype of cardiomyopathy conferred
170 by RIPK3 depletion was validated at the 2D and functional levels, and quantified routine
171 echocardiographic parameters using the M(otion)-mode (Figure 4). Compared to wild-type mice, aged
172 mdx mice are generally characterized by an eccentric hypertrophy characterized by a transiently
173 increased LV mass with increased left ventricle (LV) end-diastolic and end-systolic diameter, followed
174 by a decompensated dilated cardiomyopathy associated with a reduction LV fractional shortening and a
175 decreased LV mass (Quinlan et al., 2004a). We confirmed that our 18-month-old mdx mice suffered
176 from an eccentric hypertrophy with an increased LV mass, associated with a reduced LV internal
177 diameter in diastole (LVIDd) and systole (LVIDs) (Figure 4a-4c and Supplementary Table 1). Of note,
178 compared to mdx mice, mdx*Ripk3*$^{-/-}$ littermates displayed a 30% reduction of the LV mass, a reduction
179 of LVIDd and LVIDs that contributed to the restoration of the LV relative wall thickness value (Figure
180 4d), and unchanged fractional shortening of the LV, strain rate of cardiomyocytes from the anterior wall
181 (Figures 4e and 4f) and heart rate (Supplementary Table 1). Altogether, these data suggest that in this
182 mdx model, RIPK3-dependent necroptosis participates in the long-term development of cardiac
183 remodeling and dysfunction and that in these conditions, RIPK3 deficiency has overall cytoprotective
184 effects against dystrophic-associated cardiac deleterious phenotype.
185

186 **Discussion**

187 Necroptosis is now considered as a new therapeutic target for many degenerating disorders, including
188 cardiovascular neurodegenerative, and autoimmune diseases (Choi et al., 2021). We recently showed
189 that necroptosis is also a relevant pathogenic mechanism in myology, first by identifying the role of
190 RIPK3-dependent myonecrosis in dystrophin-deficient hindlimb muscles (Morgan et al., 2018). More
191 recently, we found that DUX4 overexpression elicits a caspase-independent, RIPK1/3-dependent cell
192 death in facioscapulohumeral dystrophy (FSHD) (Mariot et al., 2021). Clinical trials aiming at
193 pharmacologically preventing necroptosis have started but translation to neuromuscular disorders needs

194 further investigations, especially by a better understanding of the long-term consequences of necroptosis
195 inhibition in dystrophic conditions. Notably, necrotic demise affecting the diaphragm and heart are key
196 events leading to the short life expectancy of DMD boys. Whether necroptosis also mediates the
197 pathogenic phenotype in these tissues was unknown. Herein, we provide evidence that beyond its role
198 in the degeneration of locomotor muscles, necroptosis also takes part in the respiratory and cardiac
199 phenotypes in the mdx model of DMD, notably by promoting tissue fibrosis. Accumulation of
200 extracellular matrix deposition following myonecrosis is a central pathogenic process responsible for
201 the loss of function of dystrophic muscles, by progressively replacing functional muscle tissue in both
202 the myocardium and skeletal muscles (Desguerre et al., 2009). Excessive fibrosis also proportionally
203 lessens the likelihood of success for gene or cell therapies (Kharraz et al., 2014). Therefore,
204 understanding the molecular pathways directly or indirectly leading to myofibre or cardiomyocyte death
205 or fibrosis is highly relevant, accelerating the design of innovative treatments aiming at extending life
206 expectancy with improved muscle function in DMD boys.
207 An unfortunate characteristic of mouse models for DMD is the mild phenotype compared to the human.
208 Myonecrosis mainly takes place in the early phase of pathogenesis in mdx, then dramatically decreases
209 during adulthood (Muntoni et al., 1993)(Morgan et al., 2018). In contrast with human pathology, there
210 is detectable but no dramatic effect of dystrophin-deficiency on the heart and respiratory functions in
211 mdx mice. Consequently, investigating the dystrophic diaphragm and heart phenotypes requires the
212 generation of dystrophin-deficient and necroptosis-incompetent mice that would reach sufficient age to
213 progressively develop a significant phenotype (Stedman et al., 1991)(Quinlan et al., 2004b). In this
214 study, we examined the long-term effects of necroptosis inhibition, using *Ripk3* null mice, with a specific
215 focus on respiratory and cardiac muscles. As opposed to apoptosis, the execution of necrotic demise is
216 defined by an early dislocation of the plasma membrane and the release of highly inflammatory damage-
217 associated molecules pattern (DAMP) (Kroemer et al., 2009). In skeletal muscle, the permeabilization
218 of the plasma membrane also implies the passive uptake of proteins belonging to the blood compartment,
219 such as the immunoglobulins (Straub et al., 1997)(Bencze et al., 2019). Compared to young dystrophic
220 TA, the diaphragm from 18-month-old mdx mice showed IgG immunoreactivity mainly trapped in the
221 large fibrotic area (Figure 2a) and barely detected within the myofiber compartment (Figure 2c),

222 suggesting little/no ongoing myonecrosis. This was confirmed by a relative absence of active cell
223 pockets characterizing myonecrosis (Figures 2d and 2f), and only 7-8% of centrally nucleated myofibers
224 (Figure 2e). Of note, myonuclei from newly formed myofibers remain central for months, except when
225 injuries are performed in muscles from very young mice (Pastoret and Sebille, 1995). Such a low
226 percentage of central nucleation together with low cell infiltration and high fibrosis indicates that this
227 phenotype is the outcome of accumulating necrotic and regenerative events over time. Fibrosis decrease
228 was observed in the diaphragm and was associated with a decrease in the mean myofibers size and size
229 variability (Figure 2g-k). These results are consistent with a previous report assessing significant
230 myofibre cytoprotection in the diaphragm (Stupka et al., 2008). We also found a significant reduction
231 of fibrosis in the TA of old mdx*Ripk3*$^{-/-}$ (Figure 1m) compared to mdx littermates, suggesting that the
232 beneficial effects of necroptosis inhibition on muscle histology benefits both locomotor and respiratory
233 muscles.
234 Two recent studies reported that necroptosis is involved in post-lesional myogenesis (Sreenivasan et al.,
235 2020)(Zhou et al., 2020b). However, the underlying mechanisms of action of necroptosis on
236 regeneration seem unclear: Sreenivasan and colleagues observed exclusive expression of RIPK3 in mdx
237 MuSCs. They observed that mdx muscles with MuSCs depleted for RIPK3 led to a dramatic loss of
238 PAX7-expressing cells and to severely impaired muscle function, and attributed a key role of necroptosis
239 and apoptosis in mdx MuSC to sustain muscle regeneration (Sreenivasan et al., 2020). The non-apoptotic
240 roles of pro-death proteins such as caspase proteases (Fernando et al., 2002) were not discussed in this
241 study, though.
242 In line with our previous finding (Morgan et al., 2018), Zhou and colleagues found that myofibres
243 express RIPK3 and MLKL and are susceptible to necroptotic demise (Zhou et al., 2020b). They
244 demonstrated that myofibre necroptosis has a role in muscle regeneration by releasing Tenascine-C,
245 which is required for MuSCs proliferation. The authors observed an effect of myofibre necroptosis on
246 *Pax7* expression and myofiber size *in vivo* at 7 and 15 days post-injury (Zhou et al., 2020b). This work
247 did not examine the long-term effects of RIPK3- and MLKL-deficient muscle cells on myofibre size or
248 muscle function. It is therefore unclear whether necroptosis irreversibly stops or only delays
249 myogenesis. Despite their mechanistic divergences, these two studies may suggest a detrimental effect

250 of necroptosis prevention on muscle biology in a dystrophic background. Verifying whether necroptosis
251 inhibition may lead to sarcopenia of ageing regenerated muscles is therefore necessary before envisaging
252 necroptosis as a therapeutic target in muscular dystrophies.
253 In our mdx model, long-term *Ripk3* genetic depletion had no negative impact on skeletal muscle function
254 (Figure 1). While Zhou et al. focused on the role of necroptotic demise on the early steps of myogenesis
255 (which is behind the scope of our present study), our data contrast with finding of Sreenivasan and
256 colleagues on different points: First, we found no impairment of running performance in dystrophic
257 *Ripk3*$^{-/-}$ mice (Figure 1b,c), suggesting no significant reduction of muscle strength. Investigating several
258 limb muscles, we found no/little effect of RIPK3 deficiency on muscle weight, while confirming the
259 downregulation of *Ripk1* in muscle extracts (Figure 1a). EDL and TA weight were unchanged, as
260 myofibre size (Figure 1d and 1g-h), and this muscle group displayed no difference in *Pax7* and *myogenin*
261 expression in the biceps of mdx and mdx*Ripk3*$^{-/-}$, suggesting no depletion of MuSCs in mdx*Ripk3*$^{-/-}$
262 mice. Together, our results demonstrate that in mdx mice, a long-term necroptosis inhibition does not
263 lead to sarcopenia of dystrophic muscle, but rather has beneficial effects since it dampens fibrosis.
264 The lack of observed sarcopenia in our mdx*Ripk3*$^{-/-}$ dystrophic mice could be explained by a delay of
265 myogenesis when necroptosis is prevented. Zhou and colleagues only assessed a decrease of myogenesis
266 at a maximum of 15 days following an injury. Indeed, the transient inhibition of myogenesis following
267 an injury has been shown to improve the overall regenerative capacity of human MuSCs (Riederer et
268 al., 2012). Slowing down the kinetics of differentiation allows a longer proliferative phase before
269 myoblasts commitment, and ameliorates MuSC migration within the injured muscle, resulting in better
270 regeneration (Bencze et al., 2012).
271 It is also possible that any effect, positive or negative of RIPK3-deficiency on regeneration could be
272 mitigated by the cytoprotective effects of necroptosis inhibition. Not to be forgotten that the regenerative
273 process remains a consequence of previous degenerative events. Hence, the less degeneration, the less
274 resulting regeneration. Any protection against myonecrosis is therefore expected to hide any putative
275 default on regeneration.
276 Cell necrosis in dystrophin-deficient muscles does not lead to a dramatic lack of function of the limb,
277 respiratory or cardiac muscles (Partridge, 2013). Heart pathogenic phenotype becomes detectable only

278 after 10-12 months of age in mdx mice and does not lead to dramatic cardiomyopathy compared to wild-
279 type mice. However, heart weight, histological features, and analysis using M-mode echocardiography
280 can discriminate healthy from dystrophic aged hearts (Quinlan et al., 2004b)(Zhang et al., 2008)(Li et
281 al., 2009). An important finding of this study is that necroptosis depletion reduced important markers of
282 the mdx cardiomyopathy. Hearts of mdx*Ripk3*$^{-/-}$ displayed less hypertrophy and fibrosis (Figures 3 and
283 4), and this was confirmed by a significant downregulation of *Bnp* and *Myh7* transcripts that are
284 biomarkers of hypertrophic cardiomyopathy (Hasegawa et al., 1993) (Fananapazir et al., 1993). BNP
285 has been shown to be upregulated in mdx compared to C57BL/10 control mice and restored to baseline
286 in mdx mice treated by rAAV9-mediated microdystrophin (Shin et al., 2011).
287 Interestingly, some authors have observed an increase in the density of microvasculature in mdx
288 (Guéniot et al., 2016)(Latroche et al., 2015), and DMD biopsies (Miike et al., 1987). Angiogenic
289 response to myocardial infarction includes an increase in the density of CD31-positive microvessels
290 (Ren et al., 2002), and DMD patients have an increased risk for ischemic stroke (Winterholler et al.,
291 2016). A decrease of the microvasculature density as observed in our study (Figure 3d) is therefore
292 consistent with an improved heart phenotype in mdx*Ripk3*$^{-/-}$ mice. The role of canonical necroptosis has
293 been found in cardiovascular diseases, such as in atherosclerosis (Meng et al., 2015), ischemia-
294 reperfusion injuries (Smith et al., 2007) (Oerlemans et al., 2012), myocardial infarction (Luedde et al.,
295 2014), myocarditis (Zhou et al., 2018) and chemically-induced cardiomyopathy (Zhang et al., 2016).
296 Dystrophin deficiency eliciting a low-frequency dell death event, we failed to find a proper window of
297 opportunity to assess a significant decrease in cardiomyocyte demise and necroinflammation
298 (Figure 3c). However, a reduction of cardiac hypertrophy linked with a reduction of fibrosis deposition
299 suggests less accumulation of cell death events susceptible to be filled with collagen and overall
300 improved tissue homeostasis.
301
302 As a conclusion, we found that RIPK3 participates in the pathogenesis of mdx mice at different levels,
303 mediating necrosis and fibrosis accumulation in locomotor, respiratory, and cardiac muscles without
304 obvious evidence of a detrimental effect on regeneration. This study, therefore, suggests that necroptosis

305 prevention can be beneficial both to skeletal muscle and heart phenotype in DMD conditions and paves
306 the way for considering necroptosis as a therapeutic target for DMD.

307 # Material and methods

308 **Animals**

309 Mice were bred in the Institut Mondor de Recherche biomédicale, Créteil, France, and experiments on
310 mice were approved by the Anses/EnvA/Upec Ethics Committee. All care and manipulations were
311 performed by national and European legislation on animal experimentation. *Ripk3*$^{-/+}$ mice were kindly
312 provided by Genentech (San Francisco-CA). mdx*Ripk3*$^{-/-}$ mice were generated by crossing *Ripk3*$^{-/-}$ with
313 mdx mice. The resulting mice were backcrossed for at least four generations to obtain final mdx*Ripk3*$^{+/-}$
314 breeders so that analyzed mdx*Ripk3*$^{+/+}$ (mdx phenotype) and mdx*Ripk3*$^{-/-}$ mice were littermates. Only
315 males were used in this study.

316

317 **Treadmill tests**

318 The running capacity was evaluated on a treadmill (Tecmachine, Medical Development) at a +5% slope.
319 Males of 70- to 76-week-old mice were initially acclimatized to the treadmill for 5 days (10 min/day
320 and 12 m/min). Mice were challenged to an exercise of progressively increased intensity. Speed was
321 increased every 90- to 120 seconds/min and the speed of the last completed running step before
322 exhaustion was considered as the individual maximal aerobic speed.

323

324 **RNA extraction, PCR, and real-time PCR**

325 Total skeletal muscle RNA was extracted from the muscle sample using TRIzol. RNA was quantified
326 by Nanodrop. SuperScript III Reverse Transcriptase from the Invitrogen kit converted RNA into cDNA
327 using the Veriti 96- Well Fast Thermal Cycler (Applied Biosystems). Gene expression was quantified
328 by real-time qPCR with the StepOnePlus real-time PCR system (Applied Biosystems) using SYBR
329 Green detection tools (Applied Biosystems). In skeletal muscle tissue, the expression of each gene was
330 normalized to TATA Box Protein (Tbp) gene expression. Results are reported as relative gene
331 expression (2-DDCT).

332 Total heart RNA was extracted from the hearts using TRIzol® (Thermo Fisher Scientific, Saint-
333 Herblain, France) following the manufacturer's instructions. From 500 ng of extracted RNA, the first-
334 strand cDNA was then synthesized using a RevertAid First Strand cDNA Synthesis Kit (Thermo

335 Fisher Scientific, Saint-Herblain, France) with random hexamers according to the manufacturer's
336 instructions. Using the Light Cycler® 480 system (Roche Diagnostics), the reaction was carried out in
337 duplicate for each sample in a 6-µl reaction volume containing 3 µl of SYBR Green Master Mix,
338 500 nM of the forward and reverse primers each and 3 µl of diluted (1:25) cDNA. The thermal profile
339 for the SYBR Green qPCR was 95°C for 8 min, followed by 40 cycles at 95°C for 15 s, 60°C for 15 s
340 and 72°C for 30 s. The mean gene expression stability of 2 genes, *Hprt1* (*hypoxanthine-guanine*
341 *phosphoribosyl transferase 1*) and *Rpl32* (*Ribosomal protein L32*) were used as the reference
342 transcripts. Data were collected and analyzed using the LightCycler® 480 software release 1.5.0 (Roche
343 Diagnostics). Primers used in this study are the following: forward *Ripk3* 5′-
344 CGGGCACACCACAGAACAT-3′, *Ripk3* and reverse 5′- GTAGCACATCCCCAGCACCAC-3′,
345 forward *Ripk1* 5′-AGAAGAAGGGAACTATTCGC-3′ and reverse *Ripk1* 5′-
346 TTCTATGGCCTCCACGAT-3', forward *Bnp* 5'-CAGCTCTTGAAGGACCAAGG-3', reverse 5'-
347 AGACCCAGGCAGAGTCAGAA-3', forward *Myh7* 5'-AGGTGTGCTCTCCAGAATGG-3', reverse
348 5'-CAGCGGCTTGATCTTGAAGT-3', *Rpl32* - forward 5'-TGGTGAAGCCCAAGATCGTC-3',
349 reverse 5'-GGATCTGGCCCTTGAACCTT-3', *Hprt1* - forward 5'-CAGGCCAGACTTTGTTGGAT-
350 3', reverse 5'-TTGCGCTCATCTTAGGCTTT-3'
351

352 **Histology**

353 Fibrosis was labelled using Epredia Varistain Gemini ES Automated Slide Stainer. For
354 immunofluorescence: rat antibody to CD68 (clone FA-11, 137001, 1/50), rabbit antibody to mouse pan-
355 Laminin (Sigma, L9393, 1/1000), CD31anti-rat CD31 antibody (550274 clone MEC 13.3, 1/150).
356

357 **Image analysis**

358 For the analysis of the following parameters: myonecrosis, CD68-positive cells infiltrate, and fibrosis,
359 muscle and heart sections were taken from the entire length of the muscle were immunostained and
360 quantified using the ImageJ software. The section with the highest area of each measured parameter
361 (normalized to cross-section area) for each muscle is presented. Myonecrosis levels were determined
362 by measuring the area corresponding to mouse IgG uptake in myofibres (and not in interstitial areas)

363 and expressed as the percentage of the cross-sectional area. Muscle fibre minimal Feret diameter,
364 corresponding to the minimum distance between the two parallel tangents of myofibres, was determined.
365 Images analyses were performed with ImageJ by a specific self-developed macro that recognizes muscle
366 fibres as previously described (Reyes-Fernandez et al., 2019).
367
368 **Cardiac Phenotyping**
369 Mice were trained to be grasped since transthoracic echocardiography (TTE) was performed in
370 conscious, non-sedated mice to avoid any cardiac depressor effect of sedative or anaesthetic agents. Data
371 acquisition was performed every month by a single operator (JT) as previously described (Czibik et al.,
372 2021). Images were acquired from a parasternal position at the level of the papillary muscles using a 13-
373 MHz linear-array transducer with a digital ultrasound system (Vivid 7, GE Medical System, Horton,
374 Norway). Left ventricular diameters and ejection fraction, anterior and posterior wall thicknesses were
375 serially obtained from M-mode acquisition. Relative LV wall thickness (RWT) was defined as the sum
376 of septal and posterior wall thickness over LV end-diastolic diameter, and LV mass was determined
377 using the uncorrected cube assumption formula (LV mass = $(IVSd+LVIDd+PWTd)^3-LVIDd^3$). Peak
378 systolic values of radial SR in the anterior and posterior wall were obtained using Tissue Doppler
379 Imaging (TDI) as previously described (Czibik et al., 2021). TDI loops were acquired from the same
380 parasternal view at a mean frame rate of 514 fps and a depth of 1 cm. The Nyquist velocity limit was
381 set at 12cm/s. Radial SR analysis was performed offline using the EchoPac Software (GE Medical
382 Systems) by an observer (GD) blinded to the diet of the animals. The Peak systolic of radial SR was
383 computed from a region of interest positioned in the mid anterior wall and was measured over an axial
384 distance of 0.6 mm. The temporal smoothing filters were turned off for all measurements. Because slight
385 respiratory variations exist, we averaged peak systolic of radial SR on 8 consecutive cardiac cycles.
386 Hearts were harvested for histology and molecular biology.

387 # Acknowledgements

388 We thank Dr V. M. Dixit for *Ripk3* knockout mice. We also thank B. Drayton Libotte, L.
389 Guillaud and X. Decrouy for technical assistance and C. Laisne and D. Gelperowic for taking
390 good care of animals, and the VOUSH group for fruitful discussions. This work was supported

by the Association Française contre les Myopathies (AFM-Téléthon) through the Translamuscle I (#19507) and Translamuscle II (#22946) programs.

Conflict of Interest

The authors declare no conflict of interest

Bibliography

- Bencze, M., Negroni, E., Vallese, D., Yacoub-Youssef, H., Chaouch, S., Wolff, A., Aamiri, A., Santo, J.P.D., Chazaud, B., Butler-Browne, G., Savino, W., Mouly, V., Riederer, I., 2012. Proinflammatory Macrophages Enhance the Regenerative Capacity of Human Myoblasts by Modifying Their Kinetics of Proliferation and Differentiation. Molecular Therapy 20, 2168–2179. https://doi.org/10.1038/mt.2012.189
- Bencze, M., Periou, B., Baba-Amer, Y., Authier, F.J., 2019. Immunolabelling Myofiber Degeneration in Muscle Biopsies. JoVE (Journal of Visualized Experiments) e59754. https://doi.org/10.3791/59754
- Briguet, A., Courdier-Fruh, I., Foster, M., Meier, T., Magyar, J.P., 2004. Histological parameters for the quantitative assessment of muscular dystrophy in the mdx-mouse. Neuromuscul Disord 14, 675–682. https://doi.org/10.1016/j.nmd.2004.06.008
- Choi, M.E., Price, D.R., Ryter, S.W., Choi, A.M.K., 2021. Necroptosis: a crucial pathogenic mediator of human disease. JCI Insight 4, e128834. https://doi.org/10.1172/jci.insight.128834
- Czibik, G., Mezdari, Z., Murat Altintas, D., Bréhat, J., Pini, M., d'Humières, T., Delmont, T., Radu, C., Breau, M., Liang, H., Martel, C., Abatan, A., Sarwar, R., Marion, O., Naushad, S., Zhang, Y., Halfaoui, M., Suffee, N., Morin, D., Adnot, S., Hatem, S., Yavari, A., Sawaki, D., Derumeaux, G., 2021. Dysregulated Phenylalanine Catabolism Plays a Key Role in the Trajectory of Cardiac Aging. Circulation 144, 559–574. https://doi.org/10.1161/CIRCULATIONAHA.121.054204
- Desguerre, I., Mayer, M., Leturcq, F., Barbet, J.-P., Gherardi, R.K., Christov, C., 2009. Endomysial fibrosis in Duchenne muscular dystrophy: a marker of poor outcome associated with macrophage alternative activation. J Neuropathol Exp Neurol 68, 762–773. https://doi.org/10.1097/NEN.0b013e3181aa31c2
- Duan, D., Goemans, N., Takeda, S., Mercuri, E., Aartsma-Rus, A., 2021. Duchenne muscular dystrophy. Nat Rev Dis Primers 7, 1–19. https://doi.org/10.1038/s41572-021-00248-3
- Fananapazir, L., Dalakas, M.C., Cyran, F., Cohn, G., Epstein, N.D., 1993. Missense mutations in the beta-myosin heavy-chain gene cause central core disease in hypertrophic cardiomyopathy. PNAS 90, 3993–3997. https://doi.org/10.1073/pnas.90.9.3993
- Fayssoil, A., Abasse, S., Silverston, K., 2017. Cardiac Involvement Classification and Therapeutic Management in Patients with Duchenne Muscular Dystrophy. J Neuromuscul Dis 4, 17–23. https://doi.org/10.3233/JND-160194
- Fernando, P., Kelly, J.F., Balazsi, K., Slack, R.S., Megeney, L.A., 2002. Caspase 3 activity is required for skeletal muscle differentiation. PNAS 99, 11025–11030. https://doi.org/10.1073/pnas.162172899
- Gilbert, R.K., Hawk, W.A., 1963. The incidence of necrosis of muscle fibers in Duchenne type muscular dystrophy. Am J Pathol 43, 107–122.

- Guéniot, L., Latroche, C., Thépenier, C., Chatre, L., Mazeraud, A., Fiole, D., Goossens, P.L., Chrétien, F., Jouvion, G., 2016. The Female mdx Mouse: An Unexpected Vascular Story. Journal of Neurology & Neuromedicine 1.
- Hasegawa, K., Fujiwara, H., Doyama, K., Miyamae, M., Fujiwara, T., Suga, S., Mukoyama, M., Nakao, K., Imura, H., Sasayama, S., 1993. Ventricular expression of brain natriuretic peptide in hypertrophic cardiomyopathy. Circulation 88, 372–380. https://doi.org/10.1161/01.cir.88.2.372
- Kharraz, Y., Guerra, J., Pessina, P., Serrano, A.L., Muñoz-Cánoves, P., 2014. Understanding the Process of Fibrosis in Duchenne Muscular Dystrophy. BioMed Research International 2014, 1–11. https://doi.org/10.1155/2014/965631
- Khirani, S., Ramirez, A., Aubertin, G., Boulé, M., Chemouny, C., Forin, V., Fauroux, B., 2014. Respiratory muscle decline in Duchenne muscular dystrophy. Pediatr Pulmonol 49, 473–481. https://doi.org/10.1002/ppul.22847
- Kroemer, G., Galluzzi, L., Vandenabeele, P., Abrams, J., Alnemri, E.S., Baehrecke, E.H., Blagosklonny, M.V., El-Deiry, W.S., Golstein, P., Green, D.R., Hengartner, M., Knight, R.A., Kumar, S., Lipton, S.A., Malorni, W., Nuñez, G., Peter, M.E., Tschopp, J., Yuan, J., Piacentini, M., Zhivotovsky, B., Melino, G., 2009. Classification of cell death: recommendations of the Nomenclature Committee on Cell Death 2009. Cell Death Differ 16, 3–11. https://doi.org/10.1038/cdd.2008.150
- Latroche, C., Matot, B., Martins-Bach, A., Briand, D., Chazaud, B., Wary, C., Carlier, P.G., Chrétien, F., Jouvion, G., 2015. Structural and Functional Alterations of Skeletal Muscle Microvasculature in Dystrophin-Deficient mdx Mice. The American Journal of Pathology 185, 2482–2494. https://doi.org/10.1016/j.ajpath.2015.05.009
- Li, W., Liu, W., Zhong, J., Yu, X., 2009. Early manifestation of alteration in cardiac function in dystrophin deficient mdx mouse using 3D CMR tagging. J Cardiovasc Magn Reson 11, 40. https://doi.org/10.1186/1532-429X-11-40
- Luedde, M., Lutz, M., Carter, N., Sosna, J., Jacoby, C., Vucur, M., Gautheron, J., Roderburg, C., Borg, N., Reisinger, F., Hippe, H.-J., Linkermann, A., Wolf, M.J., Rose-John, S., Lüllmann-Rauch, R., Adam, D., Flögel, U., Heikenwalder, M., Luedde, T., Frey, N., 2014. RIP3, a kinase promoting necroptotic cell death, mediates adverse remodelling after myocardial infarction. Cardiovasc Res 103, 206–216. https://doi.org/10.1093/cvr/cvu146
- Mariot, V., Joubert, R., Le Gall, L., Sidlauskaite, E., Hourde, C., Duddy, W., Voit, T., Bencze, M., Dumonceaux, J., 2021. RIPK3-mediated cell death is involved in DUX4-mediated toxicity in facioscapulohumeral dystrophy. J Cachexia Sarcopenia Muscle. https://doi.org/10.1002/jcsm.12813
- Meng, L., Jin, W., Wang, X., 2015. RIP3-mediated necrotic cell death accelerates systematic inflammation and mortality. Proc Natl Acad Sci U S A 112, 11007–11012. https://doi.org/10.1073/pnas.1514730112
- Miike, T., Sugino, S., Ohtani, Y., Taku, K., Yoshioka, K., 1987. Vascular endothelial cell injury and platelet embolism in Duchenne muscular dystrophy at the preclinical stage. J Neurol Sci 82, 67–80. https://doi.org/10.1016/0022-510x(87)90007-4
- Morgan, J.E., Prola, A., Mariot, V., Pini, V., Meng, J., Hourde, C., Dumonceaux, J., Conti, F., Relaix, F., Authier, F.-J., Tiret, L., Muntoni, F., Bencze, M., 2018. Necroptosis mediates myofibre death in dystrophin-deficient mice. Nat Commun 9, 3655. https://doi.org/10.1038/s41467-018-06057-9
- Muntoni, F., Mateddu, A., Marchei, F., Clerk, A., Serra, G., 1993. Muscular weakness in the mdx mouse. Journal of the Neurological Sciences 120, 71–77. https://doi.org/10.1016/0022-510X(93)90027-V
- Newton, K., Sun, X., Dixit, V.M., 2004. Kinase RIP3 is dispensable for normal NF-kappa Bs, signaling by the B-cell and T-cell receptors, tumor necrosis factor receptor 1, and Toll-like receptors 2 and 4. Mol Cell Biol 24, 1464–1469. https://doi.org/10.1128/MCB.24.4.1464-1469.2004
- Oerlemans, M.I.F.J., Liu, J., Arslan, F., den Ouden, K., van Middelaar, B.J., Doevendans, P.A., Sluijter, J.P.G., 2012. Inhibition of RIP1-dependent necrosis prevents adverse cardiac

remodeling after myocardial ischemia-reperfusion in vivo. Basic Res Cardiol 107, 270. https://doi.org/10.1007/s00395-012-0270-8

- Partridge, T.A., 2013. The mdx mouse model as a surrogate for Duchenne muscular dystrophy. The FEBS Journal 280, 4177–4186. https://doi.org/10.1111/febs.12267
- Pastoret, C., Sebille, A., 1995. Age-related differences in regeneration of dystrophic (mdx) and normal muscle in the mouse. Muscle & Nerve 18, 1147–1154. https://doi.org/10.1002/mus.880181011
- Quinlan, J.G., Hahn, H.S., Wong, B.L., Lorenz, J.N., Wenisch, A.S., Levin, L.S., 2004a. Evolution of the mdx mouse cardiomyopathy: physiological and morphological findings. Neuromuscul Disord 14, 491–496. https://doi.org/10.1016/j.nmd.2004.04.007
- Quinlan, J.G., Hahn, H.S., Wong, B.L., Lorenz, J.N., Wenisch, A.S., Levin, L.S., 2004b. Evolution of the mdx mouse cardiomyopathy: physiological and morphological findings. Neuromuscul Disord 14, 491–496. https://doi.org/10.1016/j.nmd.2004.04.007
- Relaix, F., Bencze, M., Borok, M.J., Der Vartanian, A., Gattazzo, F., Mademtzoglou, D., Perez-Diaz, S., Prola, A., Reyes-Fernandez, P.C., Rotini, A., Taglietti, null, 2021. Perspectives on skeletal muscle stem cells. Nat Commun 12, 692. https://doi.org/10.1038/s41467-020-20760-6
- Ren, G., Michael, L.H., Entman, M.L., Frangogiannis, N.G., 2002. Morphological Characteristics of the Microvasculature in Healing Myocardial Infarcts. J Histochem Cytochem. 50, 71–79. https://doi.org/10.1177/002215540205000108
- Reyes-Fernandez, P.C., Periou, B., Decrouy, X., Relaix, F., Authier, F.J., 2019. Automated image-analysis method for the quantification of fiber morphometry and fiber type population in human skeletal muscle. Skelet Muscle 9, 15. https://doi.org/10.1186/s13395-019-0200-7
- Riederer, I., Negroni, E., Bencze, M., Wolff, A., Aamiri, A., Santo, J.P.D., Silva-Barbosa, S.D., Butler-Browne, G., Savino, W., Mouly, V., 2012. Slowing Down Differentiation of Engrafted Human Myoblasts Into Immunodeficient Mice Correlates With Increased Proliferation and Migration. Molecular Therapy 20, 146–154. https://doi.org/10.1038/mt.2011.193
- Shin, J.-H., Nitahara-Kasahara, Y., Hayashita-Kinoh, H., Ohshima-Hosoyama, S., Kinoshita, K., Chiyo, T., Okada, H., Okada, T., Takeda, S., 2011. Improvement of cardiac fibrosis in dystrophic mice by rAAV9-mediated microdystrophin transduction. Gene Ther 18, 910–919. https://doi.org/10.1038/gt.2011.36
- Smith, C.C.T., Davidson, S.M., Lim, S.Y., Simpkin, J.C., Hothersall, J.S., Yellon, D.M., 2007. Necrostatin: A Potentially Novel Cardioprotective Agent? Cardiovasc Drugs Ther 21, 227–233. https://doi.org/10.1007/s10557-007-6035-1
- Sreenivasan, K., Ianni, A., Künne, C., Strilic, B., Günther, S., Perdiguero, E., Krüger, M., Spuler, S., Offermanns, S., Gómez-Del Arco, P., Redondo, J.M., Munoz-Canoves, P., Kim, J., Braun, T., 2020. Attenuated Epigenetic Suppression of Muscle Stem Cell Necroptosis Is Required for Efficient Regeneration of Dystrophic Muscles. Cell Rep 31, 107652. https://doi.org/10.1016/j.celrep.2020.107652
- Stedman, H.H., Sweeney, H.L., Shrager, J.B., Maguire, H.C., Panettieri, R.A., Petrof, B., Narusawa, M., Leferovich, J.M., Sladky, J.T., Kelly, A.M., 1991. The mdx mouse diaphragm reproduces the degenerative changes of Duchenne muscular dystrophy. Nature 352, 536–539. https://doi.org/10.1038/352536a0
- Straub, V., Rafael, J.A., Chamberlain, J.S., Campbell, K.P., 1997. Animal Models for Muscular Dystrophy Show Different Patterns of Sarcolemmal Disruption. J Cell Biol 139, 375–385.
- Stupka, N., Schertzer, J.D., Bassel-Duby, R., Olson, E.N., Lynch, G.S., 2008. Stimulation of calcineurin Aα activity attenuates muscle pathophysiology in mdx dystrophic mice. American Journal of Physiology-Regulatory, Integrative and Comparative Physiology 294, R983–R992. https://doi.org/10.1152/ajpregu.00375.2007
- Winterholler, M., Holländer, C., Kerling, F., Weber, I., Dittrich, S., Türk, M., Schröder, R., 2016. Stroke in Duchenne Muscular Dystrophy. Stroke 47, 2123–2126. https://doi.org/10.1161/STROKEAHA.116.013678

- Zhang, T., Zhang, Y., Cui, M., Jin, L., Wang, Y., Lv, F., Liu, Y., Zheng, W., Shang, H., Zhang, J., Zhang, M., Wu, H., Guo, J., Zhang, X., Hu, X., Cao, C.-M., Xiao, R.-P., 2016. CaMKII is a RIP3 substrate mediating ischemia- and oxidative stress-induced myocardial necroptosis. Nat Med 22, 175–182. https://doi.org/10.1038/nm.4017
- Zhang, W., Hove, M. ten, Schneider, J.E., Stuckey, D.J., Sebag-Montefiore, L., Bia, B.L., Radda, G.K., Davies, K.E., Neubauer, S., Clarke, K., 2008. Abnormal cardiac morphology, function and energy metabolism in the dystrophic mdx mouse: An MRI and MRS study. Journal of Molecular and Cellular Cardiology 45, 754–760. https://doi.org/10.1016/j.yjmcc.2008.09.125
- Zhe-Wei, S., Li-Sha, G., Yue-Chun, L., 2018. The Role of Necroptosis in Cardiovascular Disease. Front Pharmacol 9, 721. https://doi.org/10.3389/fphar.2018.00721
- Zhou, F., Jiang, X., Teng, L., Yang, J., Ding, J., He, C., 2018. Necroptosis may be a novel mechanism for cardiomyocyte death in acute myocarditis. Mol Cell Biochem 442, 11–18. https://doi.org/10.1007/s11010-017-3188-5
- Zhou, S., Zhang, W., Cai, G., Ding, Y., Wei, C., Li, S., Yang, Y., Qin, J., Liu, D., Zhang, H., Shao, X., Wang, J., Wang, Hongye, Yang, W., Wang, Huating, Chen, S., Hu, P., Sun, L., 2020a. Myofiber necroptosis promotes muscle stem cell proliferation via releasing Tenascin-C during regeneration. Cell Res 30, 1063–1077. https://doi.org/10.1038/s41422-020-00393-6
- Zhou, S., Zhang, W., Cai, G., Ding, Y., Wei, C., Li, S., Yang, Y., Qin, J., Liu, D., Zhang, H., Shao, X., Wang, J., Wang, Hongye, Yang, W., Wang, Huating, Chen, S., Hu, P., Sun, L., 2020b. Myofiber necroptosis promotes muscle stem cell proliferation via releasing Tenascin-C during regeneration. Cell Res 30, 1063–1077. https://doi.org/10.1038/s41422-020-00393-6

Figures

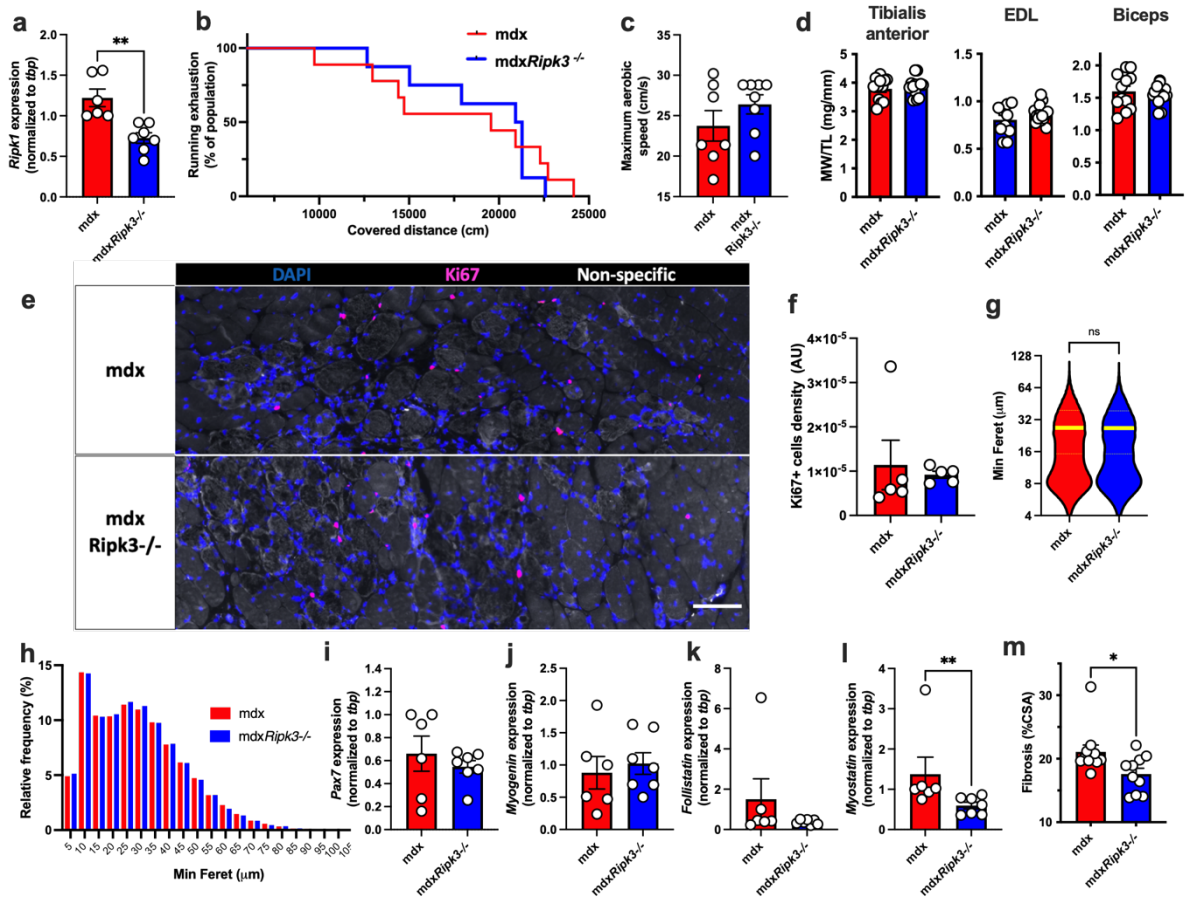

Figure 1. The genetic ablation of RIPK3 does not promote sarcopenia in 18-month-old mdx mice.

Quantification of Ripk1 transcripts in the eighteen-month-old biceps muscles (a). Seventeen-month-old mdxRipk3+/+ (i.e. mdx) and mdxRipk3-/- male mice were submitted to forced treadmill running with progressive increase of speed. (b) Endurance curve of running mice against covered distance expressed in cm. (c) Maximum aerobic speed before mice exhaustion. Data are given as means ± SEM. mdxRipk3+/+, n=7, mdxRipk3-/-, n=8. Shapiro-Wilk test followed by a Mann-Whitney test. (d) Tibialis anterior (TA), EDL and biceps muscles were harvested, and muscle weight (MW) was determined (and normalized to tibial length (MW/TL). (e) TA immunolabeling using antibodies directed against Ki67 (red). (f) Quantification of the density of Ki67-positive cells. (g) Violin plot of the pooled minimum Feret of TA myofibers (mdx: n=33,142 myofibres out of 7 distinct muscles; mdxRipk3-/-, n=26,469 myofibres out of 9 distinct muscles, Mann-Whitney test p=0.1526). (h) Relative frequencies of minimum Feret from TA myofibres are expressed in percentage. (i) Quantification of the transcript levels of Pax7, (j) myogenin, (k), follistatin and (l) myostatin in the biceps, by quantitative PCR. (m)

584 Quantification of collagen deposition using Sirius red dye. The normal distribution of data was
585 tested using the Kolmogorov-Smirnov test (passing normality test with α=0.05), leading to
586 either t-tests or Mann-Whitney tests. Data are given as means ± s.e.m.. Ns: Not significant, *:
587 p-value<0.05, **: p-value<0.01. Scale bar:100 µm
588
589

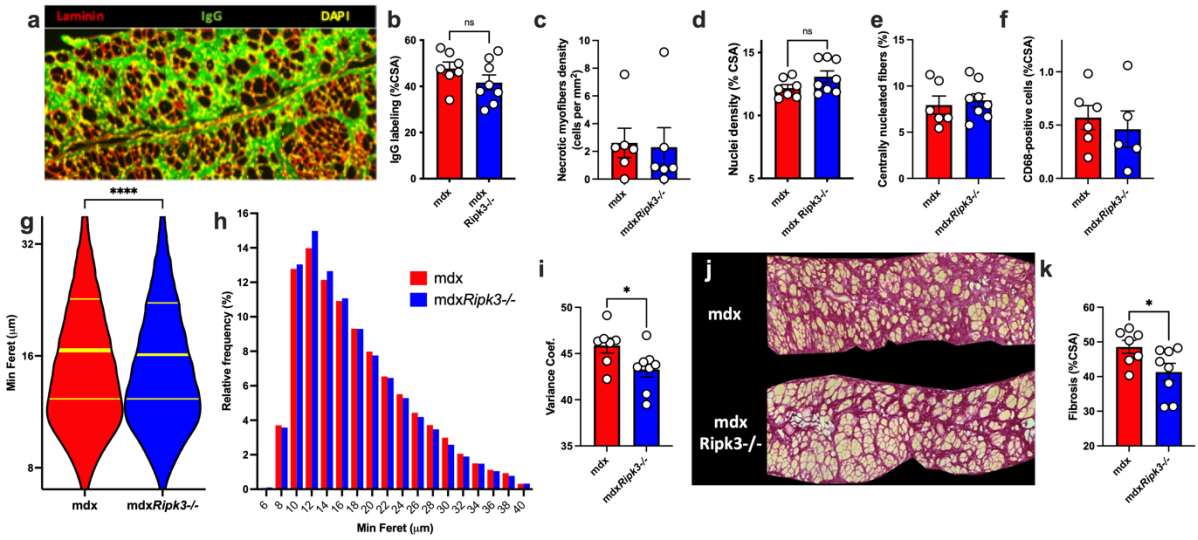

590

591 **Figure 2: Necroptosis participates in the diaphragm pathology in mdx mice.**
592 (a) Representative image of IgG uptake in diaphragms of 18-month-old mdx (mdx*Ripk3*$^{+/+}$) and
593 mdx*Ripk3*$^{-/-}$ mice. (b) Quantification of IgG uptake labelling expressed in percentage of cross-
594 sectional area (%CSA). (c) Quantification of myonecrosis extent. Myonecrosis is defined as the
595 area occupied by leaky myofibers (i.e immunoreactive for mouse IgG uptake). Quantification
596 of nuclear density expressed as a percentage of CSA (d), CD68-positive macrophage infiltrates
597 expressed in percentage of CSA (e), and centrally nucleated myofibers expressed as a
598 percentage of myofibers (f). (g) Violin plot of the minimum Ferets of diaphragm myofibers.
599 (mdx, n=16873 including 7 distinct muscles, mean:18,61±0.06555; mdx*Ripk3*-/-, n=31666
600 including 8 distinct muscles, mean:18,21±0.04554, two-tailed Mann-Whitney test p <0,0001).
601 (h) Relative frequency of minimum Ferets from diaphragm myofibers. Data are expressed as a
602 percentage. (i) Quantification of the variance coefficient of the minimum Feret of myofibers,
603 (j) representative picture of Sirius red staining (k) Quantification of diaphragm fibrosis. The
604 normal distribution of data was tested using the Kolmogorov-Smirnov test (passing normality
605 test with α=0.05), leading to either t-tests or Mann-Whitney tests. Data are given as means ±
606 s.e.m. Ns: Not significant, *: p-value<0.05, ****: p-value<0.0001.

607

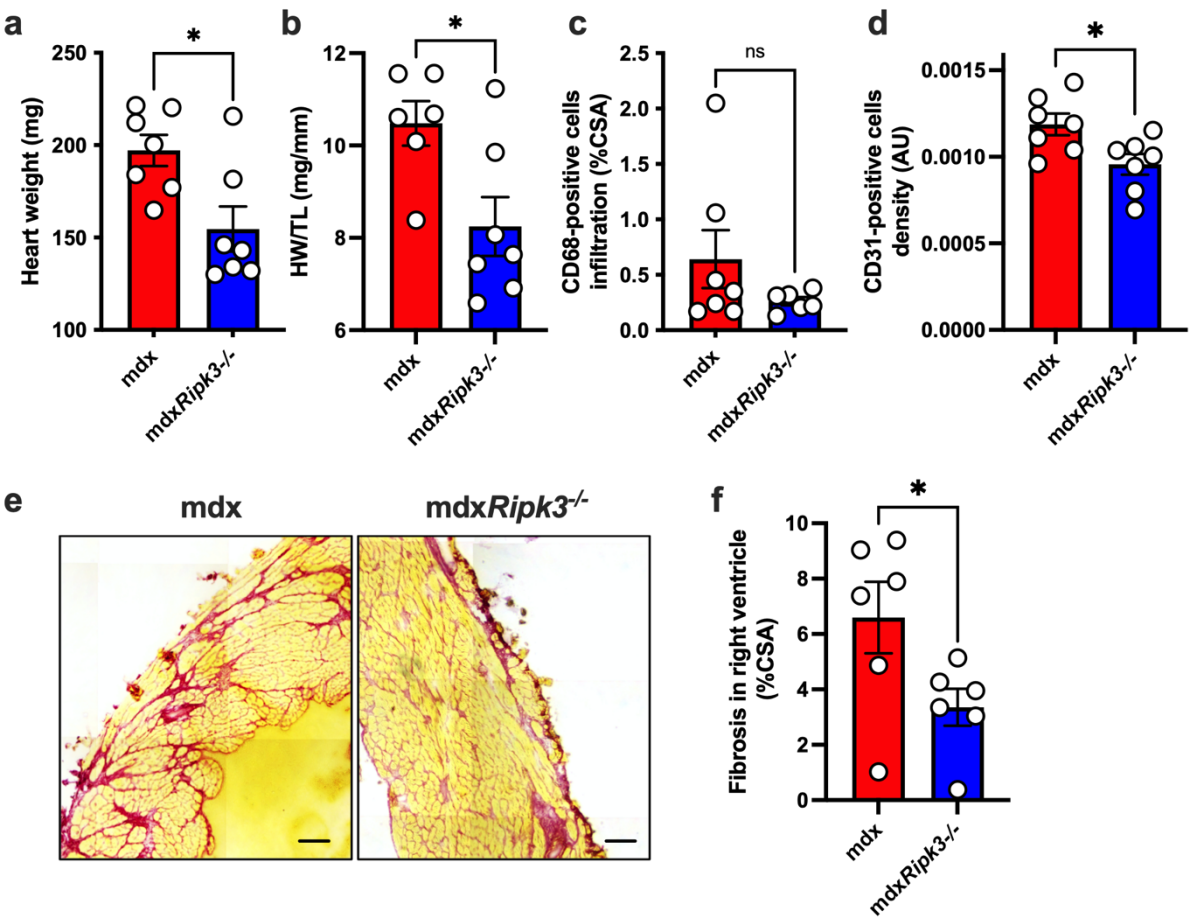

Figure 3: RIPK3 mediates heart hypertrophy in mdx mice.

(a) Heart weights of 18-month-old mdx mice. (b) Heart weight normalized to the tibial length (TL). (c) Quantification of CD68-positive macrophage infiltrates. (d) Quantification of the density of CD31-positive microvessels, (e) representative picture of Sirius red staining of right ventricles. (f) Quantification of RV fibrosis. Hearts from 18-month-old mdx*Ripk3*$^{+/+}$ and $^{-/-}$ were analyzed for *Bnp* (g), and *Myh7* (h) mRNA levels by quantitative PCR. The normal distribution of data was tested using the Kolmogorov-Smirnov test (passing normality test with α=0.05), leading to either t-tests or Mann-Whitney tests. Data are given as means ± s.e.m. Ns: Not significant, *: p-value<0.05, **: p-value<0.01. Scale bar:100µm.

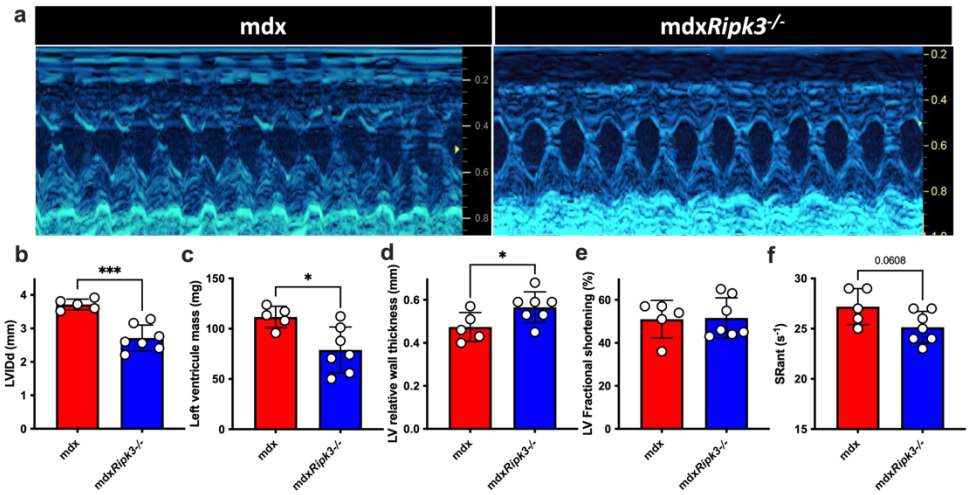

Figure 4: The genetic ablation of RIPK3 reduces cardiomyopathy in mdx mice

Representative M-mode echocardiogram traces in mdx and mdx*Ripk3*$^{-/-}$ 40-week-old mice showing a reduced left ventricle (LV) dilation in mdx*Ripk3*$^{-/-}$ mice (a). (b) Quantification of LVIDd, (c) LV mass, (d) LV relative wall thickness, (e), LV fractional shortening, and (f) strain rate (SR) of the anterior LV wall. The normal distribution of data was tested using the Kolmogorov-Smirnov test (passing normality test with α=0.05), leading to t-tests. Data are given as means ± s.e.m. *: p-value<0.05, ***: p-value<0.001.

Supplementary data

		Measured values										Calculated values			
	Mouse#	Tibial length (mm)	Normalizing factor	HR, beats/min	IVSd, mm	IVSs, mm	LVIDd, mm	LVIDs, mm	PWd, mm	PWs, mm	SRant, s-1	LV RWT, mm	LV mass, mg	LVFS, %	LVEF, %
mdx	1	21.1	0.912	523	0.78	1.45	3.81	1.85	0.74	1.68	26	0.40	95.75	51	88
	2	18.2	1.056	605	0.94	1.64	3.92	1.70	0.76	1.49	29	0.43	117.26	57	91
	3	19.2	1.006	513	0.85	1.60	3.60	1.56	0.98	1.48	27	0.51	113.44	57	91
	4	19.1	1.011	535	0.86	1.88	3.52	1.63	1.13	1.88	25	0.57	123.85	54	89
	5	18.8	1.027	605	0.85	1.13	3.72	2.38	0.85	1.31	29	0.46	108.05	36	72
	Mean	19.3	1.0	556.2	0.9	1.5	3.7	1.8	0.9	1.6	27.2	0.5	111.7	50.9	86.2
	SD	1.10	0.05	45.22	0.06	0.28	0.16	0.33	0.16	0.22	1.79	0.07	10.60	8.65	8.04
mdx*Ripk3* -:-	1	18.1	0.932	545	0.74	1.43	3.28	1.48	0.75	1.26	24	0.45	101.18	55	91
	2	17.6	0.961	503	0.89	1.75	3.16	1.11	0.78	1.53	26	0.53	112.28	65	95
	3	17.8	0.950	609	0.79	1.56	2.76	1.03	0.85	1.30	24	0.59	87.89	63	94
	4	20.7	0.816	615	0.59	1.17	2.41	1.34	0.69	1.08	27	0.53	50.19	45	82
	5	19.7	0.855	650	0.74	1.17	2.21	1.19	0.76	1.06	27	0.68	55.91	46	84
	6	19.2	0.879	640	0.76	1.22	2.60	1.46	0.78	1.17	23	0.59	74.12	44	82
	7	18.4	0.915	634	0.76	1.35	2.56	1.46	0.76	1.38	25	0.59	70.62	43	80
	Mean	18.8	0.9	599.4	0.8	1.4	2.7	1.3	0.8	1.3	25.1	0.6	78.9	51.5	86.9
	SD	1.15	0.05	54.76	0.09	0.22	0.39	0.18	0.05	0.17	1.57	0.07	22.86	9.25	6.28

Supplementary table 1: M-Mode echocardiographic values